Weak interactions in crystal engineering—understanding the recognition properties of the nitro group

James M. A. Robinson, Douglas Philp,*† Kenneth D. M. Harris and Benson M. Kariuki

School of Chemistry, University of Birmingham, Edgbaston, Birmingham, UK B15 2TT.
E-mail: dphilp@chemistry.bham.ac.uk

Received (in Cambridge, UK) 22nd May 2000, Accepted 31st July 2000
First published as an Advance Article on the web 14th September 2000

1,3,5-Trinitrobenzene and 1,3,5-triethynylbenzene cocrystallise to form a solid state structure in which the two components assemble to form segregated hydrogen-bonded tapes. This behaviour is rationalised, through the use of the Cambridge Structural Database and *ab initio* electronic structure calculations, in terms of the fundamental recognition properties of the nitro group. The recognition behaviour of the nitro group is a function of both the intrinsic electronic properties of the nitro group itself and the nature of the hydrogen bond donor with which it interacts.

Introduction

The continuing development of supramolecular chemistry and related disciplines which exploit molecular recognition relies heavily on a thorough understanding of the recognition properties of the functional groups involved in noncovalent interactions. The systematic analysis of inter- and intramolecular interactions from experimental studies in the gas, solution, and solid phases, in conjunction with computational methods, has expanded our understanding of noncovalent interactions ranging from conventional strong hydrogen bonds such as N–H···O and O–H···O to much weaker, and more subtle, interactions such as C–H···O,[1] π···π,[2] C–H···π,[3,4] and halogen–halogen.[5,6] Indeed, C–H···O interactions,[7,8] openly questioned as recently as 30 years ago, have now been shown[9] to share many of the characteristics of stronger hydrogen bonds that are formed with more conventional hydrogen bond donors such as N–H and O–H.

The observation of well-defined interaction motifs in the solid state has been rationalised using graph set analyses,[10,11] and more recently, using the concept[12] of the supramolecular synthon. However, although the qualitative descriptions provided by these approaches are evidently useful, a more quantitative understanding of the recognition properties of donor and acceptor groups is a prerequisite if we are to be able to rationalize and predict solid state structures in a routine manner.

Among studies in this field, the nitro group appears to have been underused as a hydrogen bond acceptor. In one systematic study by Etter,[13,14] the hydrogen bonding patterns resulting from contacts between amino and nitro groups in the crystal structures of nitroanilines were analysed and two important conclusions were drawn. Firstly, the potential well for the hydrogen bonds appears to be shallow, since although the hydrogens of the amino group are often within the vicinity of a nitro group, their actual positions are strongly influenced by other packing forces. Secondly, the three-centred, $R_1^2(4)$ amino–nitro interaction motifs **1** and **2** (Fig. 1a), appear to be preferred over a motif in which the hydrogen interacts with a single oxygen atom of the nitro group (**3**, Fig. 1a). By contrast, a recent combined crystallographic and computational study of X–H···O_2N interactions (where X = N and O) suggested[15] that O–H and N–H donors both favour an interaction in which only one oxygen atom interacts with the donor hydrogen atom (**3**, Fig. 1a). Interestingly, an attempt[16,17] to quantify donor and acceptor strengths in C–H···O interactions suggested that the oxygen atoms of the nitro group are much poorer hydrogen bond acceptors than oxygen atoms in other functional groups.

Other structural motifs containing nitro groups include the halogeno–nitro supramolecular synthon **4** which has been identified[18–20] in a number of crystal structures in which an iodo–nitro interaction appears to influence the overall crystal packing. We, and others, have demonstrated recently[21,22] that the halogeno–nitro synthon **4** can be evolved to the alkyne–nitro synthon **5** by virtue of the shared recognition properties[23] of terminal alkynes and organic halides (Fig. 1b and 1c). In many solid state structures containing halogeno–nitro or alkyne–nitro interactions, there appears to be a preference for the interactions to be both 3-centred and

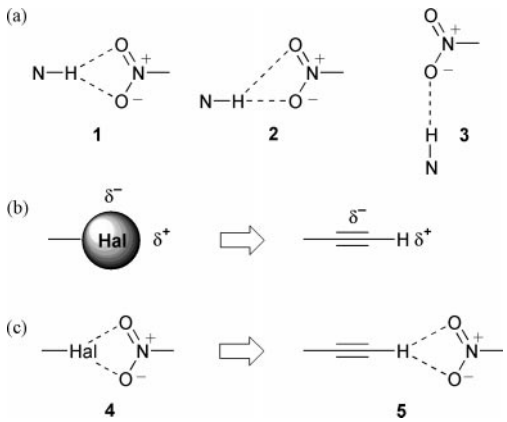

Fig. 1 (a) Three modes of interaction between N–H and nitro groups. The polarisation pattern found in terminal alkynes is similar to that for organic halides (b). Thus, the established halogen···nitro synthon **4** can be evolved into the alkynyl–nitro synthon **5** (c).

† Current address: School of Chemistry, University of St Andrews, North Haugh, St Andrews, UK KY16 9ST.

near-symmetrically bifurcated. This behaviour is further supported by a computational study[24] of C–Hal···O_2N interactions (where Hal = Cl, Br) which demonstrates that, in contrast to (stronger) X–H···O_2N interactions, C–Hal···O_2N interactions favour a symmetrically bifurcated 3-centred motif. The propensity for different types of donors (*e.g.* O–H, aniline N–H, C≡C–H and C–Hal) to adopt different interaction motifs with nitro groups is clear. The preference of a particular class of donor to form a symmetrically or non-symmetrically bifurcated $R_1^2(4)$ motif or a monocoordinated interaction should depend on the characteristics of the hydrogen bond donor. In this paper, we report an attempt to exploit the apparent propensity for terminal alkynes to participate in $R_1^2(4)$ bifurcated interactions with nitro groups in the design of an organic solid containing a hexameric hydrogen bonded array. We also describe a study of the Cambridge Structural Database (CSD) and quantum mechanical calculations which provide clear evidence that the recognition properties of the nitro group depend on the characteristics of the hydrogen bond donor.

Results and discussion

Solid state structures incorporating the alkyne–nitro synthon **5** have so far utilised either a 1,4-disubstituted benzene[22] (**6** and [**7·8**], Fig. 2) or a 4,4′-disubstituted biphenyl[21] (**9**, Fig. 2) as the scaffold on which the recognition units are located. Given the similarity between the synthons **4** and **5** and the $R_2^2(8)$ carboxylic acid dimer motif **10**, it is not surprising that the solid state structures of **6**, [**7·8**] and **9** share common packing patterns (*i.e.* the formation of hydrogen bonded tapes) with those in the solid state structure of 1,4-benzenedicarboxylic acid[25] **11**. Given this demonstration of the "interchangeability" of synthons in essentially one-dimensional hydrogen-bonded tapes, we were hopeful that the same concept could be extended to the substitution of the $R_2^2(8)$ carboxylic acid synthon **10** in two- and three-dimensional hydrogen bonded arrays with the nitro–alkyne synthon **5**.

In order to explore the extension of this concept into two dimensions, we focused on the hexameric hydrogen bonding array in the crystal structure of 1,3,5-benzenetricarboxylic acid **12** (trimesic acid[26]) and its clathrates.[27,28] It might be anticipated that the carboxylic acid dimer motif **10** in these arrays could be replaced by synthon **5**, in order to give geometrically similar arrays which exploit the (weaker) alkyne–nitro interactions. In practice, this substitution could be achieved by the replacement of the 6 trimesic acid molecules (comprising the hydrogen bonded hexamer) with 3 molecules of 1,3,5-triethynylbenzene **13** and 3 molecules of 1,3,5-trinitrobenzene **14**, with adjacent molecules interacting in the manner shown in Fig. 3.

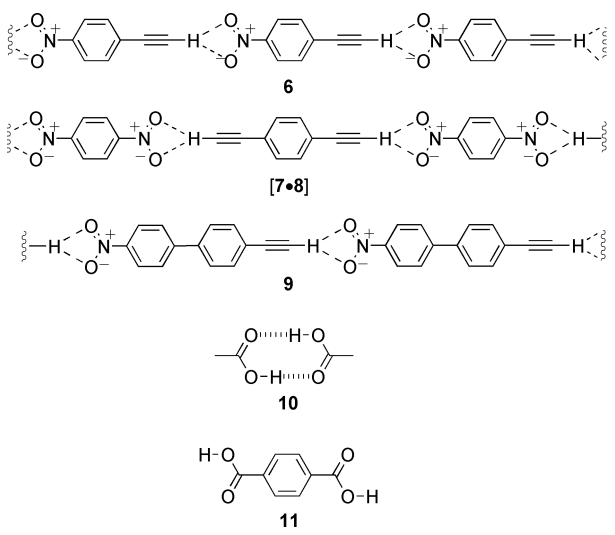

Fig. 2 One-dimensional hydrogen bonded tapes involving the alkyne–nitro synthon, and an analogous one-dimensional hydrogen bonded tape involving the carboxylic acid dimer motif **10**.

Needle-like crystals of [**13·14**] were grown by slow evaporation of 1 : 1 solutions of **13** and **14** (from a variety of solvents). In all cases, powder X-ray diffraction demonstrated that cocrystals of [**13·14**] were formed in preference to mixtures of the pure phases of **13** and **14**, suggesting that the cocrystal is favoured energetically over the pure phases. Crystals of [**13·14**] suitable for single crystal X-ray diffraction studies were grown using the method described above. The crystal structure[29] of [**13·14**] (Fig. 4a) does not contain the predicted hexameric arrays constructed from the alkyne–nitro motif **5**. Instead, the structure contains alternate tapes of **13** and **14** linked by C≡C–H···O_2N and Ar–H···O_2N contacts ($d_{H\cdots O}$ = 2.32–2.67 Å, C–H···O angles 123–157°, Fig. 4b) which are less than, or close to, the sum of the van der Waals radii[30] (Σ_{vdw} = 2.65 Å). Within the tape of molecules of **13** (Fig. 4a), there are no significant C–H···π(C≡C) interactions (shortest $d_{H\cdots C\equiv C}$ = 2.97 Å). However, within the tape of molecules of **14** (Fig. 4a), the dominant intermolecular interactions are evidently short Ar–H···O_2N contacts ($d_{H\cdots O}$ = 2.34 and 2.37 Å, C–H···O angles 154.9 and 149.1° respectively) which constitute the $R_2^2(10)$ cyclic motif [**14·14**]. The presence of the three strongly electron withdrawing nitro groups in **14** results in a relatively low pK_a (<30) for the aromatic hydrogens (*cf.* pK_a of PhH = 43). Indeed, the acidity of these protons is comparable to that for the proton of the ethynyl group (pK_a of HC≡CH = 25). This fact undoubtedly contributes to the apparent preference for the $R_2^2(10)$ motif [**14·14**] over the $R_1^2(4)$ alkyne–nitro motif **5**. The similar hydrogen bond donor abilities of these hydrogens are also reflected in the electrostatic potential (ESP) surfaces derived from HF/6-31G(d,p) *ab initio* electronic structure calculations—the maximum values

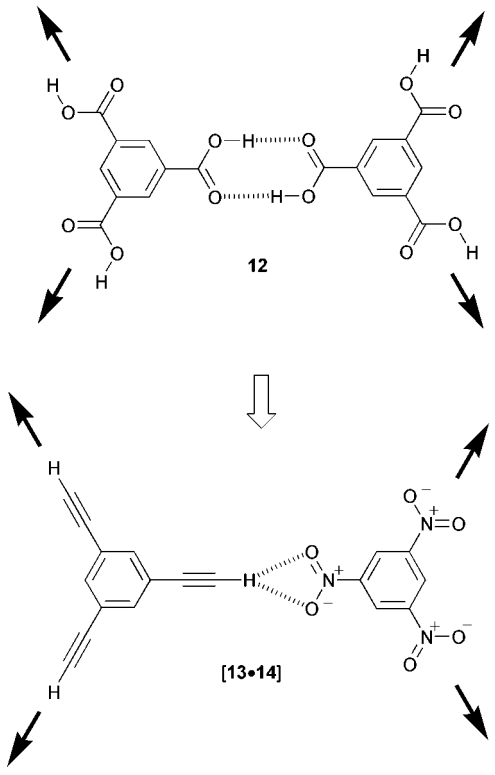

Fig. 3 In principle, the motif **12** is structurally analogous to the motif [**13·14**]. The filled arrows represent the directions of hydrogen bonding.

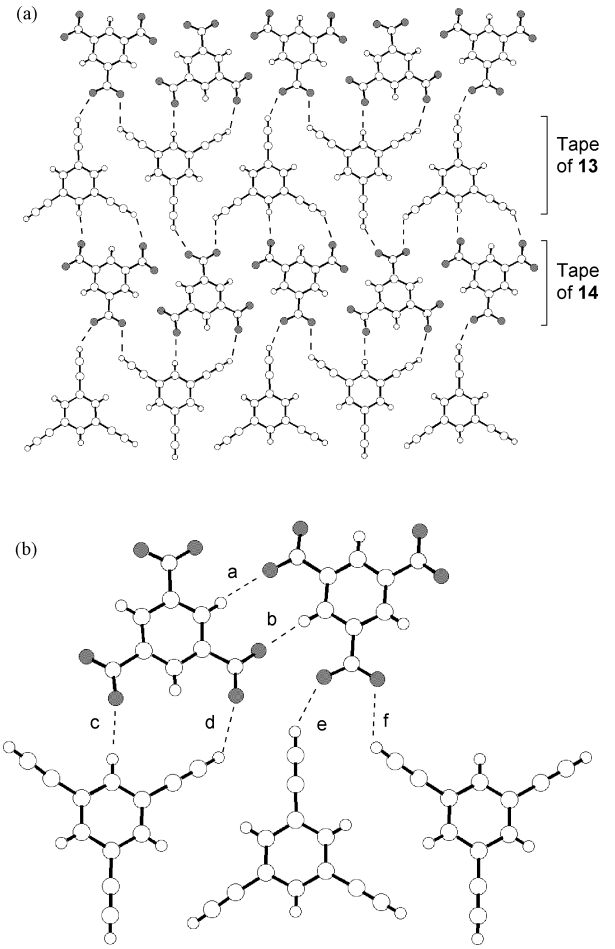

Fig. 4 (a) The structure of the cocrystal of 1,3,5-triethynylbenzene **13** and 1,3,5-trinitrobenzene **14** viewed along the *a* direction. The oxygen atoms are coloured black and the dotted lines represent C–H···O interactions. (b) The distances and angles of the C–H···O contacts are as follows: a, 2.37 Å, 149.1°; b, 2.34 Å, 154.9°; c, 2.32 Å, 156.8°; d, 2.50 Å, 130.9°; e, 2.60 Å, 139.4°; f, 2.67 Å, 123.4°.

for the ESP surface located on the Ar–H and C≡C–H hydrogens of **13** and **14**, are 204 and 173 kJ mol^{-1}, respectively.

On first inspection, it may appear surprising that molecular tapes of **14** containing the $R_2^2(10)$ motif are not present within the crystal structure[31] of **14** or many of the crystal structures in which **14** is a component. The absence of molecular tapes linked by the $R_2^2(10)$ motif within the crystal structure of **14** could be attributed to the fact that the edges of the molecular tapes bear oxygen atoms, effectively making the edges of the tapes regions of high electron density. Thus, juxtaposition of these tapes in a close packed structure would lead to electrostatic repulsion between the tape edges. Such repulsion does not exist in the structure of [**13**·**14**], since the electronegative edges are sandwiched between corresponding electropositive edges which arise from the positioning of the acidic alkyne protons along the edges of the tapes of **13**. This arrangement gives rise to the C≡C–H···O_2N interactions described above. Interestingly, the solid state structure[32] of the cocrystal formed between **14** and stilbene also contains molecular tapes of **14** in which the molecules are linked by the $R_2^2(10)$ motif. The structure of [**14**·**stilbene**] (Fig. 5) resembles that of [**13**·**14**] with the molecular tapes of **14** (electronegative edges) sandwiched between molecular tapes of stilbene (the electropositive edges of which bear relatively acidic hydrogen atoms).

However, it would be naïve to suggest that the packing of the tapes of **13** and **14** in the crystal structure of [**13**·**14**] can be rationalised simply in terms of the positioning of electronegative and weakly electropositive atoms. Other factors, such as π–π stacking and shape complementarity, must also play an

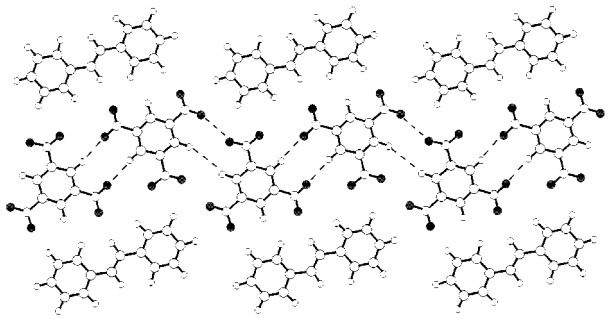

Fig. 5 A view of the structure of the cocrystal of 1,3,5-trinitrobenzene **14** and stilbene. The oxygen atoms are coloured black and the dotted lines represent C–H···O interactions between molecules of **14**.

important role. Indeed, the layers present in the solid state structure of the cocrystal [**13**·**14**] are engaged in an offset π–π stacking arrangement. Recently, we reported an investigation[23] of the role of shape complementarity in the packing of halogeno- and ethynyl-substituted benzenes in the solid state. We demonstrated that the similar packing patterns in the crystal structures of 1,3,5-substituted benzenes possessing real or (by virtue of the interchangeability of the substituents) pseudo D_{3h} symmetry can be represented by a simplistic model of tessellation involving triangular building blocks (Fig. 6a).

This model can be extended to the structure of [**13**·**14**] which has a striking resemblance to the structures of 1,3,5-halogeno-substituted benzenes, such as 1,3,5-tribromobenzene (Fig. 6b). Visual comparison of the structures reveals that the positions of the functional groups (nitro, ethynyl and bromo) form a similar pattern in both structures. Therefore, it would appear that the packing pattern observed in the [**13**·**14**] cocrystal can be rationalised both in terms of the electronic properties of the hydrogen bond donors and acceptors present and through the use of simple models based on shape complementarity. Although this empirical rationalisation is attractive, the question of the acceptor ability of the oxygen atoms

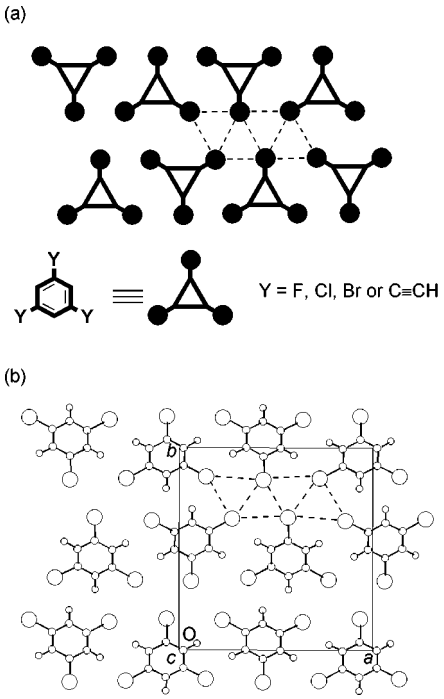

Fig. 6 (a) Schematic representation of the crystal structures of 1,3,5-trisubstituted halogenoethynylbenzenes and trihalogenobenzenes using triangular cartoons. (b) A view of the crystal structure of 1,3,5-tribromobenzene.

in the nitro group is still an open one. The oxygen atoms of the nitro group are seemingly much poorer hydrogen bond acceptors than oxygen atoms in other bonding environments, for example, C=O. An analysis[17] of the intramolecular non-covalent bonds formed between solvent molecules and oxygen hydrogen bond acceptors demonstrated that the oxygen atoms of the nitro group were poorer acceptors than the oxygen atoms in H_2O, C=O, S=O, C(sp^3)–OH and C–O–C. In fact, it was suggested that only the oxygen atoms of CO ligands attached to transition metals were poorer acceptors than nitro groups.

The degenerate resonance forms of the nitro group, each with one sp^2 hybridised oxygen participating in an N=O double bond and the other oxygen atom carrying a formal negative charge, appear to contrast with the relatively non-polar nature of the nitro group. However, a simplistic model based upon the number of available lone pairs can explain the hydrogen bond acceptor properties of a range of functional groups in which oxygen is bonded to nitrogen. Firstly, it is important to appreciate that an N=O double bond cannot be compared to a C=O double bond. Nitrogen is significantly more electronegative than carbon and so the N=O bond is undoubtedly less polarised. Secondly, it is clear that the accepting ability of oxygen atoms bonded to nitrogen depends on the number of lone pairs present on the oxygen atoms. Thus, as Fig. 7 illustrates, the oxygen atom of the nitroso group **15** has 2 lone pairs, and the two oxygen atoms of the two resonance forms of the nitro group **16** each have, on average, 2.5 lone pairs. By contrast, the oxygen atom of the nitrone **17** has only a little less than 3 (as opposed to 2.5 lone pairs), since the carbanion resonance form is only a small contributor to the ground state of the nitrone. Finally, the oxygen atom of the *N*-oxide **18** has 3 lone pairs. This trend of increasing electron density on the oxygen atom (and thus, decreasing bond order of the N–O bond) is clearly evident in the calculated (HF/6-31G(d,p)) electrostatic potential surfaces (Fig. 7). It is important to note that the presence of the negatively charged, sp^3 hybridised, oxygen in the resonance forms of the nitro group, implies that the position of the lone pairs, towards which hydrogen bonds are directed, will not necessarily be at 120° with respect to the N–O bond.

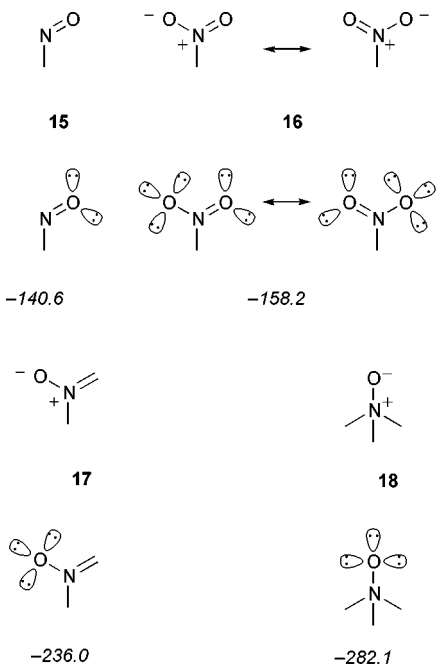

Fig. 7 Valence bond representations of functional groups which have an oxygen atom bonded to a nitrogen atom. The figures in italics are the calculated (HF/631G(d,p)) minimum values of the electrostatic potential (ESP) surfaces located on the oxygen atoms in kJ mol^{-1}.

Recent investigations of the properties of nitro groups in X–H···O_2N[15] (X = O, N) and C–Hal···O_2N[24] interactions using a combined crystallographic and quantum mechanical computational approach suggested that X–H···O_2N interactions prefer monocoordinated motifs (with X–H directed approximately towards the oxygen lone pairs), whereas C–Hal···O_2N interactions prefer a $R_1^2(4)$ symmetrically bifurcated motif. However, it must be noted that, with regard to the X–H···O_2N study, the computational investigation only considered interactions with X = O, whereas the crystallographic analysis of interactions, did not discriminate between X = O and N, and, hence, did not take account of the differences in pK_a of the donors.

Since we believe that there may be subtle, yet fundamental, variations in the recognition properties of the nitro group according to the type of hydrogen bond donor, we have performed new searches for X–H···O_2N intermolecular interactions in the Cambridge Structural Database (CSD),[33] with separate searches carried out for X = N, O and C. We appreciated that the strength, and thus classification, of these interactions depends on the bonding environment (in terms of hybridisation and charge) of the atom bearing the hydrogen atom, and so we subdivided further the hydrogen bond donors into the following six types: –O–H, $–N^+$–H, (CH)N–H, (Ar)N–H, C(sp^2)–H and C(sp^3)–H. The search of the CSD and resulting geometry calculations were performed using the QUEST3D[34] program and the results visualised using VISTA.[35] We were particularly interested in how the donor hydrogen was positioned with respect to the nitro group. Three different motifs, shown in Fig. 8, can be described as symmetrically bifurcated (**A**), bicoordinated with direction towards one of the lone pairs which are *anti* with respect to the C–N bond (**B**) and monocoordinated with direction towards the lone pair which is *syn* with respect to the C–N bond (**C**). In order to assign the interactions identified in the search to one of these three categories, two parameters were measured; the distance (denoted *d*) between the donor hydrogen atom and the nearest oxygen atom of the nitro group, and the H_{proj}···O–N angle (denoted φ), where H_{proj} denotes the position of the hydrogen atom projected on to the NO_2 plane as described[15,24] by Allen and co-workers. The angle φ is approximately +90 to +100° (depending on the distance *d*) for motif **A** and approximately +120° for motif **B**, in which H_{proj} is directed towards the lone pair which is *anti* with respect to the C–N bond. By contrast, φ is approximately −120° for the monocoordinated motif **C** in which H_{proj} is directed towards the lone pair which is *syn* with respect to the C–N bond.

The results of the searches of the CSD for X–H···O_2N intermolecular interactions with H···O distances equal to or shorter than the sum of the van der Waals[30] radii (2.65 Å) are visualised in Fig. 9. The interactions with O–H and (CH)N–H donors (Figs. 9b and 9c) both show, as expected, direction towards the probable positions of either/both of the lone pairs of the oxygen atom. Curiously, the interactions involving the best hydrogen bond donor (NH^+) show a marked preference (Fig. 9a) for the lone pair which is *syn* with respect to the C–N bond (*i.e.* motif **C**). In contrast to this preference for the *syn* lone pair, interactions involving anilines (represented by the

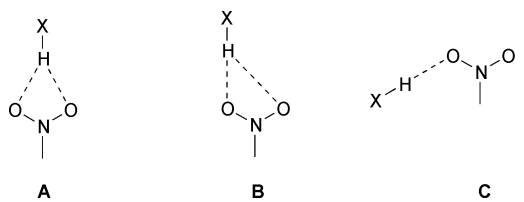

Fig. 8 Three possible modes of interaction between X–H donor groups (where X = C, N, O) and a nitro group.

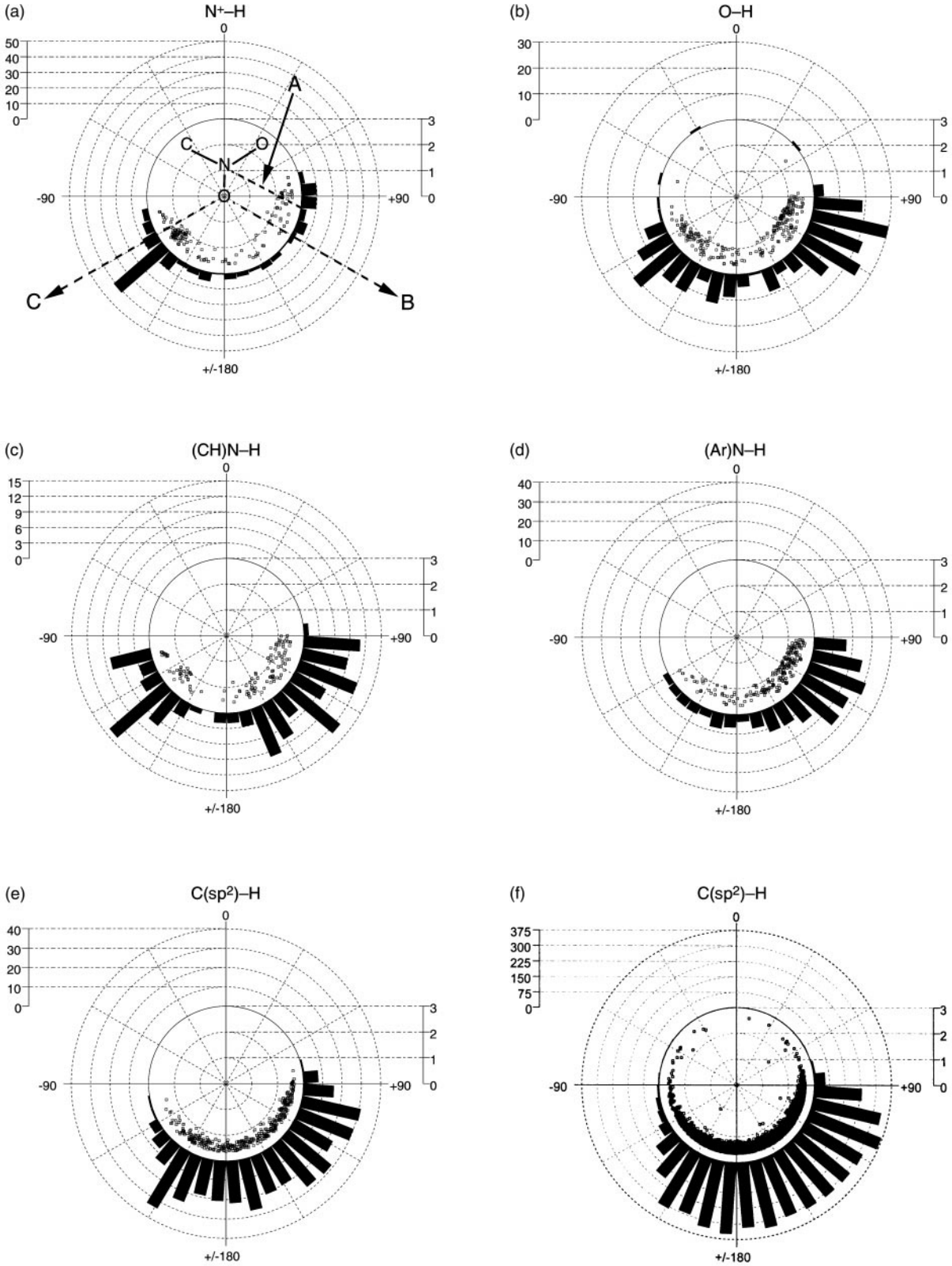

Fig. 9 Circular scattergrams showing the directionality of X–H$\cdots$O$_2$N intermolecular interactions. In all cases, H$\cdots$O distance d (radial axis) is plotted against φ (circular axis). In each plot, the right-hand vertical scale represents the distance d in Å and the left hand vertical scale represents the number of interactions which lie within a 9° interval in φ. Individual interactions are plotted as points at the coordinates (d, φ) in the inside circle of each plot and the bars in the outer circle are the total number of interactions within a 9° interval in φ. Superimposed upon plot (a) (for N^+–H) are dotted lines to represent interactions which are described by motifs **A**, **B** and **C** (Fig. 8) as well as the approximate positions of the atoms of the nitro group. The distance d (radial axis) represents the vector distance from the oxygen atom to the hydrogen atom (which is not necessarily in the C–N–O plane) as distinguished from the projected position of the hydrogen atom in the C–N–O plane which is used to determine the angle φ.

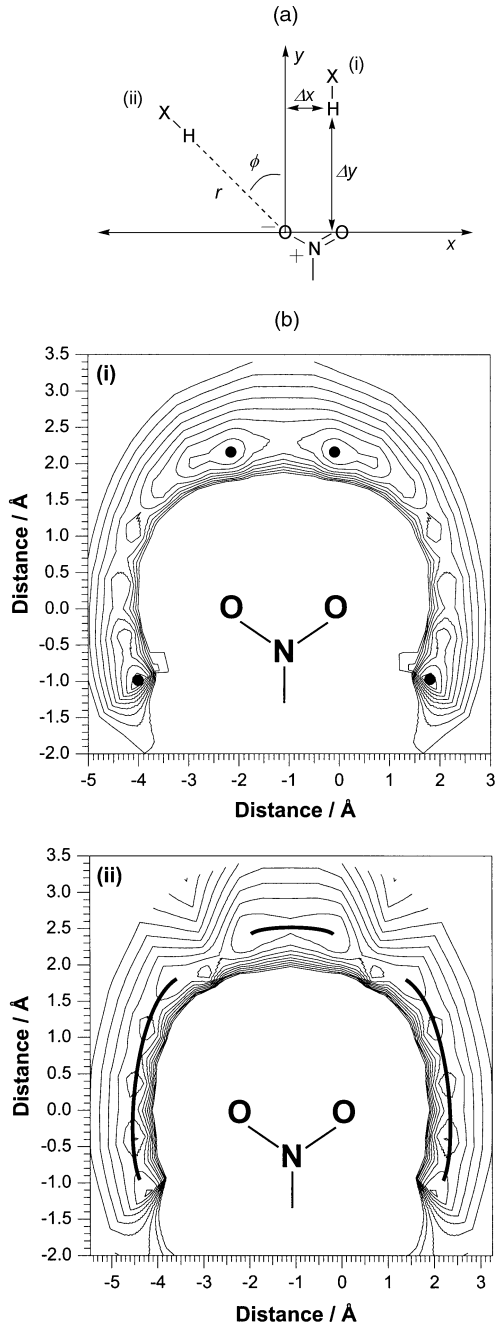

Fig. 10 (a) Coordinate system used to map the potential energy surface around the nitro group. The donor molecule HX (where X = OH or CCH) was scanned in two modes across the area around the NO_2 group. Mode (i) generated a Cartesian grid by scanning Δx from 0 to 0.7 Å in 0.1 Å steps and Δy from 1.7 Å to 3.5 Å in 0.1 Å steps. Mode (ii) generated a grid in polar coordinates, covering a radial sweep of $\phi = 0$ to 140° in 20° steps and scanning r from 1.7 Å to 3.5 Å in 0.1 Å steps. These two grids were combined to generate a complete map of the potential energy surface around the nitro group for each donor. (b) Contour maps of the potential energy surfaces around the nitro group for (i) the $[H_2O \cdot CH_3NO_2]$ complex and (ii) the $[C_2H_2 \cdot CH_3NO_2]$ complex. The vertical scales of the two contour plots are identical and the separation between contour levels in both plots is 0.1 kJ. In (i), the four dots locate the four significant minima on the potential energy surface. In (ii), the bold black curves locate the positions of the trenches discussed in the text.

(Ar)N–H donor, Fig. 9d) show a clear preference for the *anti* lone pair, although the distribution can almost certainly be attributed to the fact that many of the structures containing aromatic amino groups studied are nitroanilines for which direction of the interactions directed towards the *syn* lone pair will be sterically unfeasible. This conclusion supports Etter's observation that nitroanilines form bifurcated amino–nitro interactions of types **A** and **B**.

The extent to which the bifurcated interactions are symmetrical—*i.e.* the preference for motif **A** over motif **B**—cannot be assessed accurately from these data alone (*vide infra*) since the values of φ which characterise each motif differ by only about 20°.

Interactions involving a C(sp^2)–H donor show (Fig. 9e) only a very modest preference for direction towards the lone pairs; at best, the statistical significance of this observation is only marginal. Interactions involving a C(sp^3)–H donor (Fig. 9f) are clearly non-directional and serve as a useful reference point for the analysis of the interactions involving the better donors.

In order to probe the question of lone pair directionality in the interactions of hydrogen bond donors with the nitro group, we undertook a series of *ab initio* electronic structure calculations. These calculations map the interaction between nitromethane and a probe hydrogen bond donor. We chose a water molecule to represent a good hydrogen bond donor and an ethyne molecule to represent a poor hydrogen bond donor. Calculations were carried out on the $[H_2O \cdot CH_3NO_2]$ and $[C_2H_2 \cdot CH_3NO_2]$ complexes at the MP2/TZV(d,p) level of theory. In each case, the probe molecule was moved systematically (Fig. 10a) around the nitromethane molecule and the energy was calculated at each point on this grid. The results are presented in Fig. 10b. From the results, the preference of water to form directional hydrogen bonds to the nitro group is clearly evident. There are four potential wells, with depths greater than 4 kJ mol^{-1} [Fig. 10b (i)], at the approximate positions of the lone pairs on oxygen. Interestingly, our calculations predict that the *syn* lone pair is somewhat more basic than the lone pair *anti* to the C–N bond. By contrast, there is little evidence for any directionality in the interaction between ethyne and the oxygen atoms of nitromethane. The potential energy surface consists of a shallow trench [Fig. 10b (ii)] which encircles almost the entire region around the nitromethane oxygen atoms. From these calculations, it would appear that the directionality of the interaction is governed not only by the nature of the hydrogen bond acceptor, but also by the nature of the donor atom. For poor hydrogen bond donors, such as ethyne, the interaction is primarily van der Waals in nature and therefore lacks directionality. For good hydrogen bond donors, such as water, there is a significant electrostatic component to the interaction which gives rise to more marked directionality towards the lone pairs on oxygen.

Conclusions

It is clear that the oxygen atoms in nitro groups are relatively poor hydrogen bond acceptors (compared to oxygen atoms bonded to carbon atoms as well as nitrones and amine oxides) and may be rationalised on the basis of two factors. First, nitrogen is more electronegative than carbon, and second, the resonance forms of the nitro group imply that the oxygen atoms have fewer lone pairs of electrons than nitrones and amine oxides. These rationalisations are supported by the results presented here. We have shown that the directionality of hydrogen bonds to nitro groups is dependent on donor ability. Good donors (such as N^+–H and O–H) show a marked preference for direction towards the presumed position of the lone pairs of electrons. Poor donors (such as C–H) show no such preference. The difference, in terms in the position of the hydrogen atom, between an interaction motif which can be described as symmetrically bifurcated (*i.e.* motif **A**) and one which would be described as directed towards the lone pair of electrons *anti* to the C–N bond (*i.e.* motif **B**) is small. Thus, it is difficult, if not impossible, using analyses based upon searches of the CSD, to determine whether motif

B is predominant over motif **A**. However, it is clear from the results presented here that the recognition behaviour of the nitro group is a function of both the intrinsic electronic properties of the nitro group itself and the nature of the hydrogen bond donor with which it interacts. Thus, as the recognition properties of the nitro group depend on the hydrogen bond donor involved in the interaction, any attempt to categorise the hydrogen bonding to nitro groups in terms of a *single* type of behaviour must necessarily fail. This realisation opens the way for the development of unified models of hydrogen bonding which include quantitative descriptions of both donor and acceptor abilities.

Experimental

General

1,3,5-Triethynylbenzene was prepared according to a previously published[36] procedure and 1,3,5-trinitrobenzene was purchased from Pfaltz and Bauer. Solid state FTIR spectra were obtained from KBr disks. Spectra were also recorded from mulls in hexachloro-1,3-butadiene to discount the possibility of polymorphic interference. Solution spectra (concentration approximately 2 mM) were recorded in CCl_4 in an Aldrich Demountable liquid-cell kit with a path length of 0.5 mm. All spectra were recorded at a resolution of 2 cm^{-1} on a Perkin-Elmer Paragon 1000 spectrometer.

Computational methods

Ab initio quantum mechanical calculations (HF/6-31G(d,p)) of electrostatic potential (ESP) surfaces were performed using SPARTAN.[37] All atomic coordinates were optimised fully to a RMS gradient of less than 1×10^{-4} au.

Ab initio quantum mechanical calculations of interaction energies (MP2/TZV(d,p)), were performed using GAMESS.[38] The calculations of the potential energy surfaces of the $[H_2O \cdot CH_3NO_2]$ and $[C_2H_2 \cdot CH_3NO_2]$ complexes were performed with the same version of GAMESS.

Ab initio intermolecular perturbation (IMPT) calculations were performed using CADPAC.[39]

Cambridge Structural Database (CSD) searches

All searches reported here were of the CSD release dated January 1999 (197481 entries). The search criteria were error and disorder-free organic-only structures with *R* factors less than 7.5%. In all cases, except the search for interactions with the N^+–H donor, the heavy atom bearing the hydrogen participating in the X–H$\cdots O_2N$ interaction was constrained to have no charge. The angle φ was calculated using the LP2 parameter featured in the 3D CONSTRAIN section of QUEST.[34] Only intermolecular contacts for which the shortest X–H$\cdots$O(NO) distance was equal to or less than the sum of the van der Waals radii (2.65 Å) were considered. When the X–H$\cdots$O distances to the two oxygens of the nitro group were less than 2.65 Å, two hits were generated; one of these hits (the longer of the two) was removed manually from the data set.

Acknowledgements

This work was supported by grants from the Engineering and Physical Sciences Research Council (to B. M. K. and J. M. A. R.) and from the University of Birmingham.

References

1 (*a*) Z. Berkovitch-Yellin and L. Leiserowitz, *Acta Crystallogr., Sect. B*, 1984, **40**, 159; (*b*) G. R. Desiraju, *Acc. Chem. Res.*, 1996, **29**, 441.
2 (*a*) G. R. Desiraju and A. Gavezzotti, *Acta Crystallogr., Sect. B*, 1989, **45**, 473; (*b*) C. V. Sharma, K. Panneerselvam, T. Pilati and G. R. Desiraju, *J. Chem. Soc., Perkin Trans. 2*, 1993, 2209; (*c*) C. A. Hunter, *J. Mol. Biol.*, 1993, **230**, 1025.
3 For discussions concerning C–H$\cdots\pi$(Ar) interactions, see: (*a*) G. R. Desiraju and A. Gavezzotti, *J. Chem. Soc., Chem. Commun.*, 1989, 621; (*b*) C. A. Hunter and J. K. M. Sanders, *J. Am. Chem. Soc.*, 1990, **112**, 5525; (*c*) C. A. Hunter, *Chem. Soc. Rev.*, 1994, **23**, 101; (*d*) D. R. Boyd, T. A. Evans, W. B. Jennings, J. F. Malone, W. O'Sullivan and A. Smith, *Chem. Commun.*, 1996, 2269.
4 For discussions concerning C–H$\cdots\pi$(C≡C) interations, see: (*a*) T. Steiner, *J. Chem. Soc., Chem. Commun.*, 1995, 95; (*b*) T. Steiner, E. B. Starikov, A. M. Amado and J. J. C. Trixeria-Dias, *J. Chem. Soc., Perkin Trans. 2*, 1995, 1321; (*c*) T. Steiner, M. Tamm, A. Grzegorzewski, N. Schulte, N. Veldman, A. M. M. Schreurs, J. A. Kanters, J. Kroon, J. van der Maas and B. Lutz, *J. Chem. Soc., Perkin Trans. 2*, 1996, 2441.
5 J. A. P. R. Sarma and G. R. Desiraju, *Acc. Chem. Res.*, 1986, **19**, 222.
6 G. R. Desiraju and R. Parthasarathy, *J. Am. Chem. Soc.*, 1989, **111**, 8725.
7 T. Steiner, J. van der Maas and B. Lutz, *J. Chem. Soc., Perkin Trans. 2*, 1997, 1287.
8 B. M. Kariuki, K. D. M. Harris, D. Philp and J. M. A. Robinson, *J. Am. Chem. Soc.*, 1997, **119**, 12679.
9 For recent discussions of the properties of C–H$\cdots$O interactions, see: (*a*) T. Steiner, *Chem. Commun.*, 1997, 727; (*b*) T. Steiner and G. R. Desiraju, *Chem. Commun.*, 1998, 891.
10 M. C. Etter, *Acc. Chem. Res.*, 1990, **23**, 120.
11 J. Bernstein, R. E. Davis, L. Shimoni and N. L. Chang, *Angew. Chem., Int. Ed. Engl.*, 1995, **34**, 1555.
12 For a recent discussion of the term "supramolecular synthon", see: A. Nangia and G. R. Desiraju, *Top. Curr. Chem.*, 1998, **198**, 57.
13 T. W. Panunto, Z. Urbánczyk-Lipkowska, R. Johnson and M. C. Etter, *J. Am. Chem. Soc.*, 1987, **109**, 7786.
14 M. C. Etter, K. S. Huang, G. M. Frankenbach and D. A. Adsmond, *ACS Symp. Ser.*, 1991, **455**, 446.
15 F. H. Allen, C. A. Baalham, J. P. M. Lommerse, P. R. Raithby and E. Sparr, *Acta Crystallogr., Sect. B*, 1997, **53**, 1017.
16 T. Steiner, *J. Chem. Soc., Chem. Commun.*, 1994, 2341.
17 T. Steiner, *New J. Chem.*, 1998, **22**, 1099.
18 F. H. Allen, B. S. Goud, V. J. Hoy, J. A. K. Howard and G. R. Desiraju, *J. Chem. Soc., Chem. Commun.*, 1994, 2729.
19 V. R. Thalladi, B. S. Goud, V. J. Hoy, F. H. Allen, J. A. K. Howard and G. R. Desiraju, *Chem. Commun.*, 1996, 401.
20 J. A. R. P. Sarma, F. H. Allen, V. J. Hoy, J. A. K. Howard, R. Thaimattam, K. Biradha and G. R. Desiraju, *Chem. Commun.*, 1997, 101.
21 P. J. Langley, J. Hulliger, R. Thaimattam and G. R. Desiraju, *New J. Chem.*, 1998, **22**, 1307.
22 J. M. A. Robinson, D. Philp, B. M. Kariuki and K. D. M. Harris, *Chem. Commun.*, 1999, 329.
23 J. M. A. Robinson, B. M. Kariuki, K. D. M. Harris and D. Philp, *J. Chem. Soc., Perkin Trans. 2*, 1997, 2459.
24 F. H. Allen, J. P. M. Lommerse, V. J. Hoy, J. A. K. Howard and G. R. Desiraju, *Acta Crystallogr., Sect. B*, 1997, **53**, 1006.
25 M. Bailey and C. J. Brown, *Acta Crystallogr.*, 1967, 22.
26 D. J. Duchamp and R. E. Marsh, *Acta Crystallogr., Sect. B*, 1969, **25**, 5.
27 F. H. Herbstein, in *Comprehensive Supramolecular Chemistry*, ed. J. L. Attwood, J. E. D. Davies, D. D. MacNicol and F. Vögtle, Elsevier, Oxford, 1996, vol. 6, pp. 61–83.
28 S. V. Kolotuchin, E. E. Fenlon, S. R. Wilson, C. J. Loweth and S. C. Zimmerman, *Angew. Chem., Int. Ed. Engl.*, 1995, **34**, 2654.
29 Crystal data for [**13**·**14**] at 296(2) K: $[C_6H_3N_3O_6 \cdot C_{12}H_6]$, $M = 363.28$, monoclinic, space group $P2_1/c$, $a = 7.3724(10)$, $b = 14.696(3)$, $c = 15.930(2)$ Å, $\beta = 92.334(8)^\circ$, $V = 1724.5(4)$ Å^3, $Z = 4$, $D_c = 1.399$ g cm^{-3}, $\lambda = 1.5406$ Å, $\mu = 0.920$ mm^{-1}, $F(000) = 744$. A brown needle-like crystal of dimensions $0.30 \times 0.20 \times 0.15$ mm was used. Data were measured on a Rigaku R-AXIS II rotating anode/image plate diffractometer using graphite-monochromated Cu-Kα radiation. 1448 independent reflections were measured ($6.86 \leqslant 2\theta \leqslant 51.22^\circ$, $R_{(int)} = 0.065$), of which 1337 were considered to be observed, $R = 0.060$, $wR_2 = 0.160$. CCDC reference number 440/203. See http://www.rsc.org/suppdata/nj/b0/b004086j/ for crystallographic files in .cif format.
30 R. S. Rowland and R. Taylor, *J. Chem. Phys.*, 1996, **100**, 7384.
31 C. S. Choi and J. E. Abel, *Acta Crystallogr., Sect. B*, 1972, **28**, 193.
32 I. Bar and J. Bernstein, *Acta Crystallogr., Sect. B*, 1978, **34**, 3438.

33 (*a*) F. H. Allen and O. Kennard, *Chem. Des. Automat. News*, 1993, **8**, 1; (*b*) F. H. Allen and K. O. Kennard, *Chem. Des. Automat. News*, 1993, **8**, 31.
34 Cambridge Structural Database, *User's Manual. Getting Started with the CSD System*, Cambridge Crystallographic Centre, 1994.
35 Cambridge Structural Database, *VISTA2.0 User's Manual Getting Started with the CSD System*, Cambridge Crystallographic Centre, 1995.
36 T. X. Neenan and G. M. Whitesides, *J. Org. Chem.*, 1988, **53**, 2489.
37 SPARTAN, Wavefunction, Inc., Irvine, CA, 1997, version 4.1.1.
38 M. W. Schmidt, K. K. Baldridge, J. A. Boatz, S. T. Elbert, M. S. Gordon, J. H. Jensen, S. Koseki, N. Matsunaga, K. A. Nguyen, S. J. Su, T. L. Windus, M. Dupuis and J. A. Montgomery, *J. Comput. Chem.*, 1993, **14**, 1347. The version dated 8th May 1998 was used in all calculations.
39 CADPAC, The Cambridge Analytical Derivatives Package, Issue 6.5, University of Cambridge, 1998.